


Regulatory Effects of Damaged Renal Epithelial Cells After Repair by *Porphyra yezoensis* Polysaccharides with Different Sulfation Degree on the Calcium Oxalate Crystal–Cell Interaction

Xin-Yuan Sun ^{1,*}Hui Zhang^{2,*}Ji-Wang Deng^{1,*}Bang-Xian Yu¹Yi-Han Zhang¹Jian-Ming Ouyang ²

¹Department of Urology, Guangzhou Institute of Urology, Guangdong Key Laboratory of Urology, The First Affiliated Hospital of Guangzhou Medical University, Guangzhou Medical University, Guangzhou, Guangdong, 510230, People's Republic of China;

²Department of Chemistry, Institute of Biomineralization and Lithiasis Research, Jinan University, Guangzhou, 510632, People's Republic of China

*These authors contributed equally to this work

Correspondence: Xin-Yuan Sun
Department of Urology, Guangzhou Institute of Urology, Guangdong Key Laboratory of Urology, The First Affiliated Hospital of Guangzhou Medical University, Guangzhou Medical University, Guangzhou, Guangdong, 510230, People's Republic of China
Email sunxinyuan1985@163.com

Jian-Ming Ouyang
Department of Chemistry, Institute of Biomineralization and Lithiasis Research, Jinan University, Guangzhou, 510632, People's Republic of China
Tel +86-20-85223353
Email toyjm@jnu.edu.cn

Background: The interaction between urinary microcrystals and renal epithelial cells is closely related to kidney stone formation. However, the mechanism of cell state changes that affect crystal–cell interaction remains unclear.

Methods: This study investigated the relationship between the sulfate group ($-\text{OSO}_3^-$) content in *Porphyra yezoensis* polysaccharide (PYP) and the ability to repair damaged cells, as well as the changes in cell adhesion and endocytosis of nano-calcium oxalate monohydrate (COM) crystals before and after PYP repair of damaged renal tubular epithelial cells. The sulfur trioxide–pyridine method was used to sulfate PYP ($-\text{OSO}_3^-$ content of 14.14%), and two kinds of sulfated PYPs with $-\text{OSO}_3^-$ content of 20.28% (SPYP1) and 27.14% (SPYP2) were obtained. The above three PYPs were used to repair oxalate-damaged human proximal tubular epithelial cells (HK-2), and the changes in the biochemical indicators of the cells before and after the repair and the changes in cell adhesion and endocytosis of nano-COM crystals were detected.

Results: After repair by PYPs, the cell viability increased, the number of reactive oxygen species decreased, and the reduction of mitochondrial membrane potential and the release of intracellular Ca^{2+} were suppressed. The cells repaired by PYPs inhibited the adhesion of nano-COM crystals while promoting the endocytosis of the adhered crystals. The endocytosed crystals mainly accumulated in the lysosome. The ability of PYPs to repair cell damage, inhibit crystal adhesion, and promote crystal endocytosis was enhanced when the $-\text{OSO}_3^-$ content increased. Among them, SPYP2 with the highest $-\text{OSO}_3^-$ content showed the best biological activity.

Conclusion: SPYP2 showed the best ability to repair damaged cells, followed by SPYP1 and PYP. SPYP2 may become a potential green drug that inhibits the formation and recurrence of calcium oxalate stones.

Keywords: *Porphyra yezoensis* polysaccharide, polysaccharide sulfation, cell repair, adhesion and endocytosis, kidney stone

Introduction

Hyperoxaluria is one of the main risk factors for idiopathic calcium oxalate (CaOx) stones.¹ Oxalate is a metabolic end product and the main component of most clinically detected CaOx renal stones. High concentrations of oxalate exposed on the surface of renal epithelial cells can cause a large amount of reactive oxygen species (ROS) production, destroy mitochondrial function, and cause oxidative

damage to cells.² In addition, oxalate can increase the release of lactate dehydrogenase (LDH) and the levels of hydrogen peroxide (H₂O₂) and prostaglandin E2 (PGE2),³ leading to oxidative damage to the cells.

Crystal–cell interaction (adhesion and endocytosis) is an important process for the formation of CaOx kidney stones. Lieske et al⁴ co-cultured a ¹⁴C-labeled calcium oxalate monohydrate (COM) crystal with kidney epithelial cells of monkey origin (BSC-1) cells and found that the COM crystal adhered to the microvilli on the cell surface. The COM crystal was endocytosed, transferred to the lysosomes in approximately 30 min, and decomposed under the action of many hydrolases. This rapid uptake reduces the nucleation sites of crystallites on the cell surface, which is a self-protection mechanism of cells. Lieske et al⁵ indicated that COM crystals can stimulate DNA synthesis and promote cell proliferation and growth after being phagocytized by MDCK cells. Some researchers also showed that the damage to renal epithelial cells will promote the adhesion and reduce the endocytosis of crystals.⁶ This is because damaged cells promote the over-expression of adhesion proteins, such as hyaluronic acid (HA), osteopontin (OPN), CD44, and annexin A2.⁷ Meanwhile, a large amount of adenosine-triphosphate (ATP) is required for cell endocytosis, and the ability of damaged cells to synthesize ATP is weakened, which reduces the phagocytosis of cells to the crystal, thereby intensifying the adhesion and aggregation of crystals on the cell surface.⁸ Zhao et al⁹ found that oxalate-induced damage to HK-2 cells causes phosphatidylserine (PS) eversion and increases the expression of OPN, leading to increased adhesion of nano-COM crystal. However, when damaged cells are repaired by polysaccharides, the expression of PS and OPN is reduced, and the adhesion of crystals on the cell surface is decreased. Cell swallow crystals is an active transportation process that requires energy consumption. After cell damage, the ability to synthesize ATP and endocytosis capacity decrease,¹⁰ which cause crystals to stay in the kidneys, thereby increasing the risk of kidney stones.

Seaweed polysaccharides have strong antioxidant activity and low cytotoxicity, which have attracted the attention of researchers.¹¹ *Porphyra yezoensis* is a seaweed that widely grows along the coast of Southeast Asian countries. *P. yezoensis* polysaccharide (PYP) is the main component of *P. yezoensis*, which has many biological activities such as antioxidant and anticoagulant activities.¹² In our previous

study, low-molecular-weight PYP was found to have a good repair effect on oxalate-damaged cells.¹³

The biological activity of polysaccharides is closely related to their molecular weight and sulfate group (–OSO₃[–]) content.¹⁴ Polysaccharides with a higher –OSO₃[–] content show stronger antioxidant activity.¹⁵ Ma et al¹⁶ found that four kinds of degraded seaweed polysaccharides (DSPs, with –OSO₃[–] content of 17.9%, 13.3%, 8.2%, and 5.5%) had obvious repair effects on damaged HK-2 cells. After DSP repair, the cell membrane integrity was increased, and LDH release and cell apoptosis and necrosis rate were significantly decreased. The DSP with the highest –OSO₃[–] content (17.9%) had the strongest repair ability. Wang et al¹⁷ extracted three polysaccharides with –OSO₃[–] contents of 23.30% (F1), 36.41% (F2), and 36.67% (F3) from laminarin. With the highest –OSO₃[–] content, F3 showed the best ability to scavenge superoxide radicals, followed by F2 and F1.

The biological activities of polysaccharides are directly affected by their structure and physicochemical properties, especially for their molecular weights (Mws) and active group content. In our previous study,¹⁸ we investigated the relationship between molecular weights (Mws) of PYP and cell protection ability. Four degraded fractions, namely, PYP1, PYP2, PYP3, and PYP4, were successfully obtained, with Mws of 576.2, 49.5, 12.6, and 4.02 kDa, respectively. PYP protection reduced the crystal toxicity and inhibited the adhesion and endocytosis of HK-2 cells by nano-COM. With decreasing molecular weight, the ability of PYP to reduce cell damage and inhibit cell adhesion and endocytosis increased. In the present study, a PYP with a –OSO₃[–] content of 14.14% was sulfated by sulfur trioxide–pyridine, and two kinds of sulfated PYPs with –OSO₃[–] contents of 20.28% and 27.14% were obtained. To reveal the internal relationship between cell status and the formation of kidney stones, the ability of these polysaccharides to repair oxalate-damaged HK-2 cells and the effects of these cells before and after repair on the adhesion and endocytosis of nano-COM were investigated.

Materials and Methods

Materials and Apparatus

Materials

Natural *P. yezoensis* polysaccharide (PYP) was provided by Shanxi Ciyuan Biotechnology Co., Ltd. The polysaccharide content of PYP was 95%. According to our previous study,¹⁹ COM crystal with the size of 100 nm

were prepared, the physicochemical properties of prepared crystals were characterized by XRD analysis, FT-IR analysis and SEM observation. HK-2 cells were purchased from the Shanghai Cell Bank of the Chinese Academy of Sciences (Shanghai, China). Fluo-4/AM and Lyso-Tracker Red were purchased from Shanghai Beyotime Bio-Tech Co., Ltd. (Shanghai, China). Cell counting kit (CCK-8) was purchased from Dojindo Laboratory (Kumamoto, Japan). Hematoxylin-eosin (HE) staining kits were purchased from Shanghai Beyotime Bio-Tech Co., Ltd. (Shanghai, China). Annexin V-FITC/Propidium iodide (PI) was purchased from Beijing 4A Biotech Co., Ltd. (Beijing, China). 5',6,6-tetrachloro-1,1',3,3'-tetraethyl-imidacarbocyanine iodide (JC-1) and 2',7'-dichlorodihydrofluorescein diacetate (DCFH-DA) were purchased from Becton, Dickinson and Company, USA. Primary antibodies against the following proteins were used in this study: CD44 (#ab24504, 1:1000) and Annexin A2 (#ab185957, 1:1000) were purchased from Abcam, β -tubulin rabbit pAb (#AC008, 1:5000) and GAPDH mouse mAb (#AC002, 1:10000) were purchased from ABclonal Technology. The following secondary antibodies used in this study were purchased from LI-COR Biosciences: IRDye 800CW goat anti-mouse IgG (926–32210, 1:10000), IRDye 800CW goat anti-rabbit IgG (926–32211, 1:10000).

Apparatus

Fourier transform infrared spectrometer (FT-IR, EQUINOX 55, Bruker, Germany), confocal laser scanning microscope (LSM510 Meta Duo Scan, Zeiss, Germany), inverted fluorescence microscope (Leica Dmra2, Germany), microplate reader (Safire2, Tecan, Männedorf, Switzerland), flow cytometer (FACS Aria, BD Corporation, Franklin Lakes, NJ, USA), ULTRA 55 field emission scanning electron microscope (Zeiss company, Germany), optical microscope (Olympus, Ckx41, Japan), transmission electron microscope (TEM) (H-7650, Hitachi, Japan).

Experimental Methods

Preparation of *P. yezoensis* Polysaccharide (PYP)

Samples of *P. yezoensis* were collected from the Fujian of China from August to September 2019. The material was sorted, washed and dried immediately by forced air circulation at 50–60°C. PYP was obtained from algal powder of *P. yezoensis* by a hot water-extracted method according to our previous study.^{8,13,20}

Sulfation of PYP

According to the reference,²¹ 500 mg of PYP with a $-\text{OSO}_3^-$ content of 14.14% and 30 mL dimethyl sulfoxide were added to three-necked flask and stirred at room temperature for 1 h. Subsequently, the temperature was raised to 80°C, 5 g of sulfur trioxide-pyridine dissolved in 5 mL of anhydrous formamide was added, and the reaction was carried out for 8 h and 16 h, then cooled to room temperature and neutralized with NaOH. Dialysis was carried out in distilled water with 3000 M dialysis bag until the polysaccharide solution changed from yellow to transparent, and then alcohol precipitation for 24 h at 4°C. Sulfated PYP with content of $-\text{OSO}_3^-$ content of 20.28% (SPYP1) and 27.14% (SPYP2) were obtained after centrifugation and drying.

Determination of $-\text{OSO}_3^-$ Content in Polysaccharides

BaCl₂-gelatin turbidimetry was used to determine the $-\text{OSO}_3^-$ in polysaccharides.²² A standard curve was plotted through a series of known concentrations of K₂SO₄, the standard working curve: $Y=2.21289X-0.01095$; $R^2=0.99449$; $n=11$. Based on the regression equation, the $-\text{OSO}_3^-$ content in polysaccharide was calculated.

FT-IR and NMR Detection of Polysaccharides

FT-IR spectra of polysaccharides were determined using films prepared by the dried polysaccharides and KBr pellets on a Fourier-transform infrared spectrophotometer in the wave number range of 4000–400 cm^{-1} with a resolution of 4 cm^{-1} .

For NMR analysis, approximately 20 mg of freeze-dry PYP sample was dissolved in 0.5 mL of deuterium oxide in NMR tube (5 mm diameter), and analysis was performed using a Varian Bruker-600 MHz spectrophotometer.

Cell Culture

HK-2 cells were grown in DMEM/F-12 medium supplemented with 10% fetal bovine serum and penicillin–streptomycin antibiotics at 37°C under an atmosphere of 95% air and 5% CO₂.

Cell Viability Detection by CCK-8 Kit

After the cell culture was completed, the cells were divided into three groups: (1) normal control group: serum-free medium was added; (2) damaged control group: 2.6mM sodium oxalate dissolved in PBS buffer solution was added to damage HK-2 cells for 3.5 h; (3) polysaccharide repair group: PYP and sulfated PYP (SPYP1 and SPYP2) with the concentrations of 20, 40, 60 and 100 $\mu\text{g}/\text{mL}$ were

added to the damaged cells for repairing 12 h. 10 μ L CCK-8 were added to each well and incubated for 1.5 h. The absorbance was detected by a microplate reader at 450 nm, and cell viability was calculated.

Cell Morphology Observation

2 mL of cell suspension with a concentration of 1×10^5 cells/mL was inoculated per well in 6-well plates at 37°C for 24 h. The cells were divided into three groups: (1) normal control group: serum-free medium was added; (2) oxalate injury group: 2.6mM sodium oxalate dissolved in PBS buffer solution was added to damage HK-2 cells for 3.5 h; (3) polysaccharide repair group: PYP, SPYP1 and SPYP2 with the concentration of 20, 40, 60 and 100 μ g/mL were added to repair damaged cells for 12 h. The cells were then observed under a microscope.

Detection of Reactive Oxygen Species (ROS) Level

After the PYPs repair for damaged cells was completed, 500 μ L DCFH-DA staining solution diluted with a serum-free culture medium at 1:1000 was added and incubated for 30 min at 37°C. ROS distribution was observed under fluorescent microscope. The fluorescence intensity of intracellular ROS was quantitatively detected by a microplate reader at 502 nm.

Intracellular Ca^{2+} Level Detection

After the PYPs repair for damaged cells was completed, the cells were fixed by 3.7% paraformaldehyde solution at room temperature for 10 min, and then stained with 200 μ L of Fluo-4/AM (5 μ mol/L) and incubated for 45 min. DAPI staining solution was then added to the cells and incubated for additional 10 min. The prepared samples were mounted with an anti-fade fluorescence mounting medium and observed in a confocal microscope.

Detection of Mitochondrial Membrane Potential

After the PYPs repair for damaged cells was completed, the cells were stained by 5 μ g/mL JC-1 staining solution at 37°C for 1 h. The mitochondrial membrane potential was observed and detected with an inverted fluorescence microscope and flow cytometry.

Western Blotting Assay

After the PYPs repair for damaged cells was completed, the cells were washed 3 times with PBS, and the supernatant was completely drained. Cell lysates were prepared using lysis buffers supplemented with phosphatase and protease inhibitors. Equal amounts of protein were loaded and separated on 12% SDS-PAGE, and then transferred to

polyvinylidene fluoride (PVDF) membrane. The membrane was then blotted by incubation overnight with transmembrane protein (CD44) and Annexin A2 primary antibodies. Images were obtained with an Odyssey[®] CLx Imaging System (LI-COR, USA) and quantified using Image J software.

Detection of the Proportion of Cells with Adherent Crystals

Preparation of fluorescence labeled nano-COM crystals: According to the method reported by Zhao et al,²³ the nano-COM was labeled with FITC, and FITC-COM was prepared by a two-step reaction. First, AMPTES (5 mL) was reacted with COM (0.05 g) and absolute ethanol (50 mL) at 74°C for 3 h. Subsequently, 0.025 g of FITC was supplemented, and the reaction was maintained for 6 h. Fluorescence-labeled COMs were harvested followed by washing and drying.

After the PYPs repair for damaged cells was completed, the cells were transferred to a 4°C environment for cultivation for 30 min to inhibit the endocytic activity of cells. The experiment was divided into 3 groups: (1) control group: 200 μ g/mL freshly prepared FITC-labeled COM was added to normal HK-2 cells; (2) injury group: 200 μ g/mL freshly prepared FITC-labeled COM was added to oxalate damaged HK-2 cells; (3) repair group: 200 μ g/mL freshly prepared FITC-labeled COM were added to PYPs repaired cells. Then, the three groups of cells were transferred to 4°C for 1 h. After the culture time was reached, the culture medium was aspirated and washed twice with cold PBS to remove the unattached and non-tightly adherent crystals. After the trypsin digestion, the cells were resuspended in PBS, and the average fluorescence intensity and the proportion of cells with adherent crystals were measured by a flow cytometer. Cells with FITC signal could be considered as cells with adherent crystals.

SEM Observation

After the PYPs repair for damaged cells was completed, 200 μ g/mL COM crystals with the size of about 100 nm were added and inculcated for 6 h, the supernatant was removed by suction and cells were washed three times with PBS, fixed in 2.5% glutaraldehyde at 4°C for 24 h, then fixed with 1% OsO₄, washed three times with PBS, dehydrated in gradient ethanol (30%, 50%, 70%, 90% and 100%, respectively), dried under the critical point of CO₂, treated with gold sputtering, and finally imaged on SEM.

Detection of the Proportion of Cells with Endocytosed Crystals

Cells were divided into three groups according to Detection of the Proportion of Cells with Adherent Crystals. After incubation for 6 h at 37°C, the cells were washed with PBS and incubated with 5 mM EDTA for 10 min to eliminate non-internalized (both adherent and non-adherent crystals) COM crystals.²⁴ The internalized crystals were then quantified using a flow cytometer. Cells with an FITC signal, as detected by flow cytometry, can be regarded as cells with endocytosed crystals. The X-axis indicates the relative intensity of the fluorescence signal. The strength of the FITC signal represents the amount of endocytosed crystals.

Accumulation of Nano-COM Crystals in Lysosomes

Cells were divided into three groups according to Detection of the Proportion of Cells with Adherent Crystals. The cells were stained with 70 nM Lyso-Tracker Red to label lysosomes for 2 h and then fixed with 4% paraformaldehyde for 10 min, the cell nucleus was stained with DAPI. Accumulation of COM crystals in lysosomes was observed by confocal laser scanning microscope.

Statistical Analysis

Statistical analyses were performed using the SPSS 13.0 software. Data were expressed as the mean \pm SD. Multiple group comparisons were performed using one-way ANOVA, followed by the Tukey post hoc test. If $p < 0.05$, there was a significant difference; if $p < 0.01$, the difference was extremely significant; and if $p > 0.05$, there was no significant difference.

Results

Sulfation and Structural Characterization of PYPs

Sulfation of PYP

PYP was sulfated by sulfur trioxide–pyridine to obtain two sulfated polysaccharides (SPYP1 and SPYP2; Table 1). With prolonged sulfation time, the $-\text{OSO}_3^-$ content of

polysaccharides increased from 14.11% (PYP) to 20.28% (SPYP1) and 27.14% (SPYP2).

FT-IR Characterization

The FT-IR spectrum (Figure 1B) shows that the PYP spectra before and after sulfation are similar, indicating that sulfation with sulfur trioxide–pyridine did not remarkably influence the overall structure of polysaccharides. These PYPs have obvious broad peaks around 3412–3445 cm^{-1} , corresponding to the stretching vibration of O–H; the absorption peak at 2933 cm^{-1} is due to C–H telescopic vibration.²⁵

However, sulfated polysaccharide has strong absorption bands near 1250 and 817 cm^{-1} , which are the characteristic absorption peaks of the asymmetric stretching vibrations of the sulfate groups O=S=O and C–O–S.²⁶ The intensity of the peaks (1250 and 817 cm^{-1}) gradually increases with the increase in sulfation time (Figure 1B), indicating that the content of $-\text{OSO}_3^-$ in polysaccharides gradually increased.

¹H NMR and ¹³C NMR Characterization

Our previous study¹³ found that PYP has a typical porphyrin structure and a backbone of alternating (1 \rightarrow 3)-linked β -D-galactose units and (1 \rightarrow 4)-linked 3,6-anhydro- α -L-galactose or (1 \rightarrow 4)-linked- α -L-galactose 6-sulfate units.²⁷

The structures of PYP before and after sulfation were further characterized by ¹H NMR and ¹³C NMR analysis. After sulfation, a strong signal peak appeared at δ 4.21 ppm, which was the reason that the chemical shift of δ 4.45 and δ 4.58 ppm shifted to δ 4.21 ppm after sulfation. This may be due to the fact that $-\text{OSO}_3^-$ replaced $-\text{OH}$ after sulfation.²⁸ In the ¹³C NMR spectrum, a new peak appeared at δ 66.96 ppm because the carbon atoms connected by the $-\text{OSO}_3^-$ group shifted to low frequency,²⁸ indicating that the C6 position of G is substituted by the $-\text{OSO}_3^-$ (Table 2). After sulfation, the $-\text{OH}$ at C2, C4, and C6 positions in (1 \rightarrow 3)-linked β -D-galactose of PYP were partially replaced by the $-\text{OSO}_3^-$. These results showed that the sulfation of PYP was successful.²⁰

Table 1 Sulfation Conditions and Chemical Properties of Original and Sulfated *P. yezoensis* Polysaccharides

Sample	Reaction Time t/h	$-\text{OSO}_3^-$ Content/% (Mean \pm SD)	Coefficient of Variation/%	Characteristic Absorption Peaks of Groups/ cm^{-1}			
				$-\text{OH}$	$-\text{CH}_2$	O=S=O	C–O–S
PYP	0	14.14 \pm 0.12	0.83	3412	2933	1248	820
SPYP1	8	20.28 \pm 0.73	3.60	3421	2949	1249	822
SPYP2	16	27.14 \pm 0.65	2.41	3445	2949	1250	820

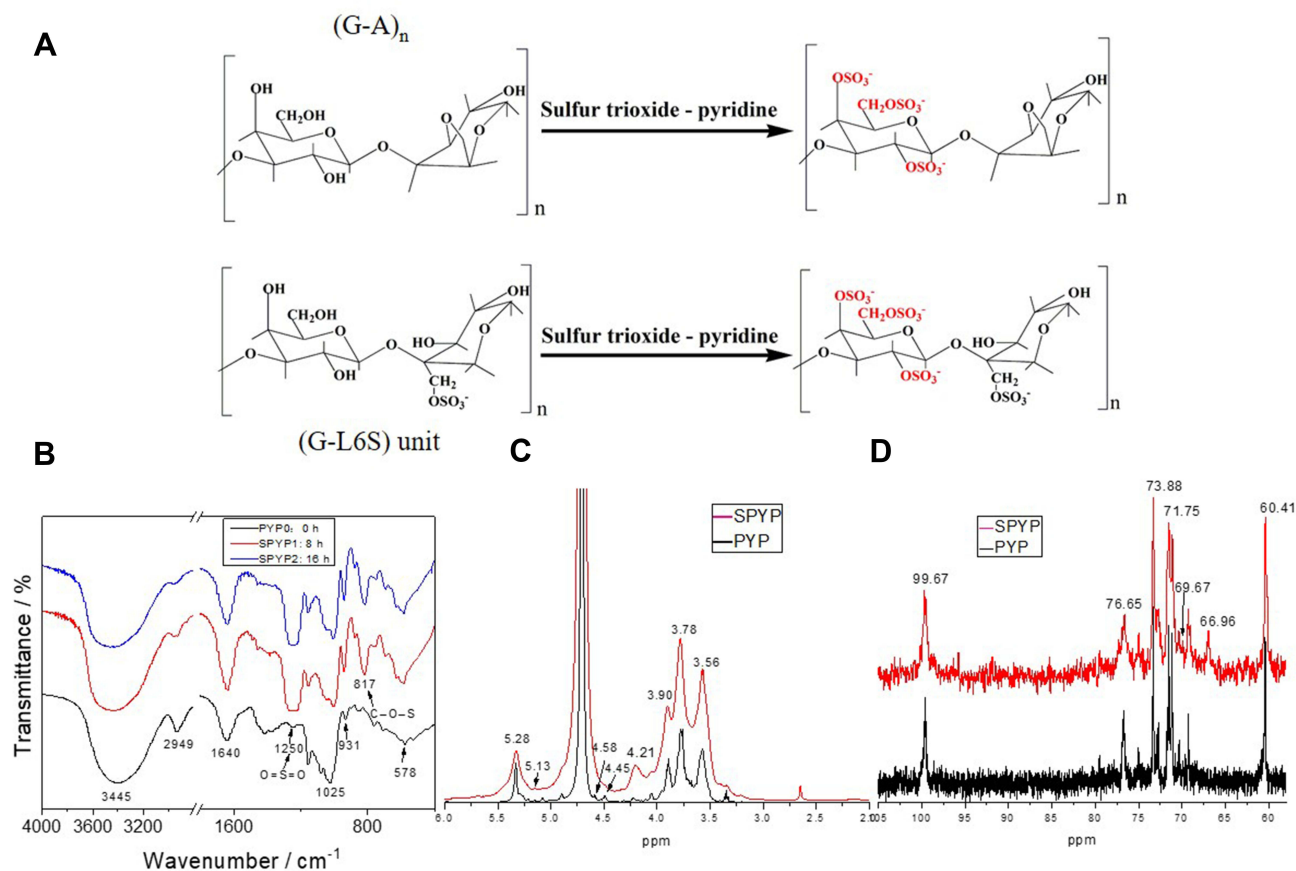


Figure 1 Schematic diagram of sulfation reaction and chemical properties characterization of PYPs before and after sulfation. **(A)** Schematic diagram of sulfation reaction; **(B)** FT-IR spectra; **(C)** ^1H NMR spectra; **(D)** ^{13}C NMR spectra.

PYPs Improved the Viability of Injured HK-2 Cells

As shown in Figure 2A, the cell viability decreased from $100\% \pm 0.81\%$ to $59.49\% \pm 1.34\%$ after oxalate-induced

injury, indicating that oxalate has obvious damage to cells. When 20, 40, 60, and 100 $\mu\text{g}/\text{mL}$ of PYP, SPYP1, and SPYP2 were used to repair the damaged HK-2 cells, the cell viability increased to different degrees (69.35–

Table 2 The ^{13}C NMR Chemical Shift Data of PYP Before and After Sulfation

	Residue	^{13}C Chemical Shift (ppm)												
		C-1	C-1 [#]	C-2	C-2 [#]	C-3	C-3 [#]	C-4	C-4 [#]	C-5	C-5 [#]	C-6	C-6 [#]	
PYP	(G-A) _n	G	102.92		71.47		82.35		68.34		75.06		60.37	
		A	99.58		71.01		79.56		76.34		76.07		69.52	
	(G-L6S) unit	G	103.18		69.91		81.52		69.29		76.67		60.46	
		L6S	101.89		69.27		71.72		78.61		70.27		67.50	
SPYP	(G-A) _n	G	102.67	-	71.66	73.88	82.35	-	68.90	69.67-	75.06	-	60.40	66.96
		A	99.71	-	70.83	-	79.38	-	76.39	-	75.97	-	69.51	-
	(G-L6S)unit	G	103.83	-	70.27	71.75	81.52	-	69.29	70.25-	76.60	-	60.47	66.96
		L6S	100.73	-	69.27	-	71.65	-	78.61	-	70.36	-	67.52	-

Notes: [#]Indicates the ^{13}C NMR chemical shift of PYP after sulfation; G: (1→3)-linked β -D-galactose; A: (1→4)-linked 3,6-anhydro- α -L-galactose; L6S: (1→4)-linked- α -L-galactose 6-sulfate.

91.26%), with 100 $\mu\text{g/mL}$ concentration showing the best repair effect. Therefore, a concentration of 100 $\mu\text{g/mL}$ was selected for the following experiments.

With a polysaccharide concentration of 100 $\mu\text{g/mL}$, the cell viability increased from 81.16% to 86.25% and 91.26% when the polysaccharide $-\text{OSO}_3^-$ content was increased from 14.14% (PYP) to 20.28% (SPYP1) and 27.14% (SPYP2), respectively. This finding shows that the sulfated polysaccharides SPYP1 and SPYP2 have stronger repair ability than the unsulfated PYP, and the higher the $-\text{OSO}_3^-$ content, the greater the cell viability.

PYPs Restored the Cell Morphology of Oxalate-Damaged HK-2 Cells

The morphological changes of HK-2 cells before and after PYP repair with different $-\text{OSO}_3^-$ content were observed under a microscope (Figure 2B). Normal cells are fully shaped and tightly connected. After the cells were damaged by oxalate, the cell morphology became disordered and shrunk, and the number was obviously reduced. When the damaged cells were repaired by PYP, SPYP1, and SPYP2, the cells gradually returned to normal state. Among them, SPYP2 with the highest $-\text{OSO}_3^-$ content had the best repair effect.

PYPs Reduced the Production of Intracellular ROS

As shown in Figure 3A, the green fluorescence of normal cells is the weakest (5821 ± 225); that is, the ROS level is the lowest. By contrast, the green fluorescence of ROS in

damaged cells is obviously increased ($12,809 \pm 250$). After repair with polysaccharides, the ROS level gradually decreased with the increase of $-\text{OSO}_3^-$ content of polysaccharides (7745–6080, Figure 3B). SPYP2, which has the highest degree of sulfation, effectively eliminated ROS in the cells.

PYPs Decreased the Intracellular Ca^{2+} Level

The increase of intracellular free Ca^{2+} concentration may disturb the mitochondrial membrane potential ($\Delta\psi\text{m}$) and eventually lead to cell apoptosis and necrosis. Fluo-4 AM was used as a fluorescence probe to detect intracellular Ca^{2+} level (Figure 4A and B). The green fluorescence intensity of normal cells was weak, whereas that of damaged cells was obviously increased. In the polysaccharide repair groups, the fluorescence intensity of intracellular Ca^{2+} decreased with the increase of $-\text{OSO}_3^-$ content in polysaccharides. The fluorescence intensity in the SPYP2-repaired group was close to the normal group.

PYPs Recovered Mitochondrial Membrane Depolarization

Cell oxidative damage can lead to decreased $\Delta\psi\text{m}$. When $\Delta\psi\text{m}$ decreases, fluorescent probe JC-1 changes from red fluorescence (aggregate) to green fluorescence (monomer). The normal cells have strong red fluorescence intensity, whereas the oxalate-damaged cells show strong green fluorescence (Figure 5A and B). The red fluorescence of the repaired cells gradually increased, and the green

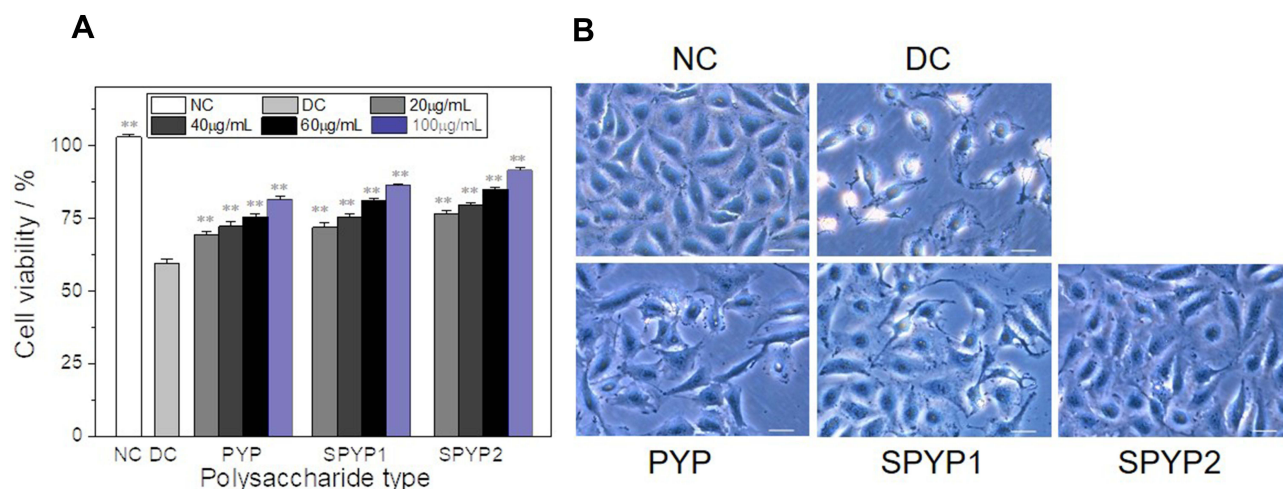


Figure 2 Changes of viability (A) and morphologies (B) of damaged cells before and after repair by PYPs with different $-\text{OSO}_3^-$ content. Polysaccharide concentration: 20, 40, 60, and 100 $\mu\text{g/mL}$; oxalate concentration: 2.6 mmol/L; injury time: 3.5 h; repair time: 12 h. Compared with DC group, $**P < 0.01$. Scale bars: 20 μm . **Abbreviations:** NC, normal control; DC, damaged control.

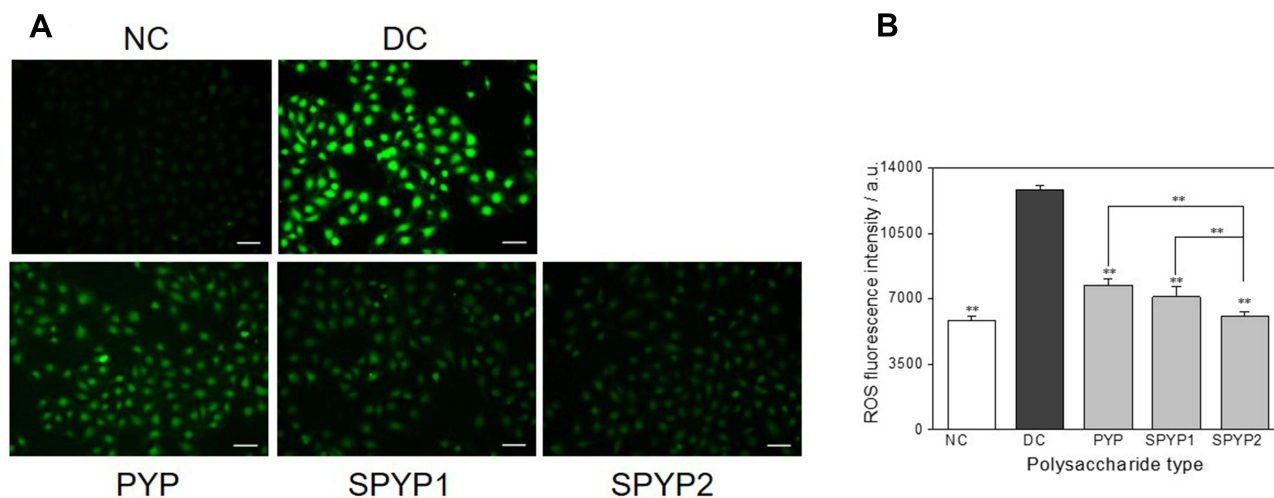


Figure 3 Intracellular ROS expression of damaged cells before and after repair by PYPs with different $-\text{OSO}_3^-$ content. **(A)** Fluorescence microscopy images; **(B)** quantitative histogram of fluorescence intensity. Polysaccharide concentration: 100 $\mu\text{g}/\text{mL}$; oxalate concentration: 2.6 mmol/L ; injury time: 3.5 h; repair time: 12 h. Compared with DC group, $**P < 0.01$. Scale bars: 50 μm .

Abbreviations: NC, normal control; DC, damaged control.

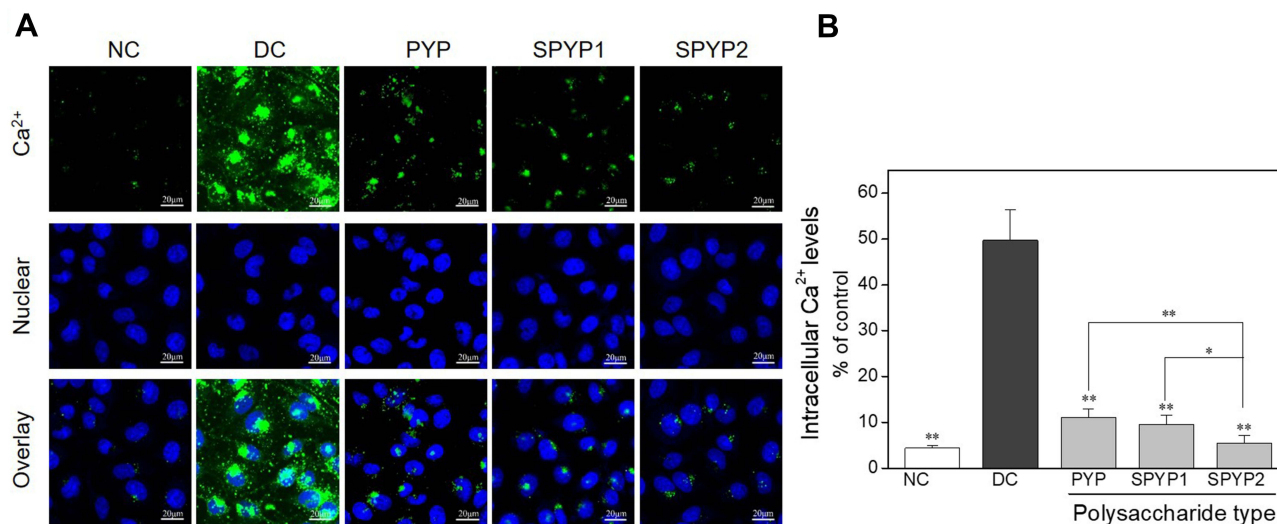


Figure 4 Changes of intracellular Ca^{2+} levels of damaged cells before and after repair by PYPs with different $-\text{OSO}_3^-$ content. **(A)** Fluorescence microscopy images; **(B)** quantitative histogram of fluorescence intensity. Polysaccharide concentration: 100 $\mu\text{g}/\text{mL}$; oxalate concentration: 2.6 mmol/L ; injury time: 3.5 h; repair time: 12 h. Compared with DC group, $*P < 0.05$; $**P < 0.01$. Scale bars: 20 μm .

Abbreviations: NC, normal control; DC, damaged control.

fluorescence decreased (Figure 5C and D), indicating that the repair effect of sulfated polysaccharides (SPYP1 and SPYP2) on damaged cells is obviously enhanced than that before sulfation (PYP).

PYPs Inhibited the Expression of Adhesion Proteins

When renal epithelial cells are damaged, many molecules and proteins can be expressed on their surfaces, such as transmembrane protein (CD44),⁷ HA,²⁹ and

annexin A2.³⁰ These negatively charged adhesion proteins provide an effective adhesion site for urinary microcrystals and promote the formation of early microlithiasis.³¹

Compared with that in the normal group, the expression of CD44 and annexin A2 in the injured group was obviously increased (Figure 6A and B). Oxidative damage resulted in the overexpression of cell surface adhesion proteins. After polysaccharide repair, the expression of the three adhesion proteins

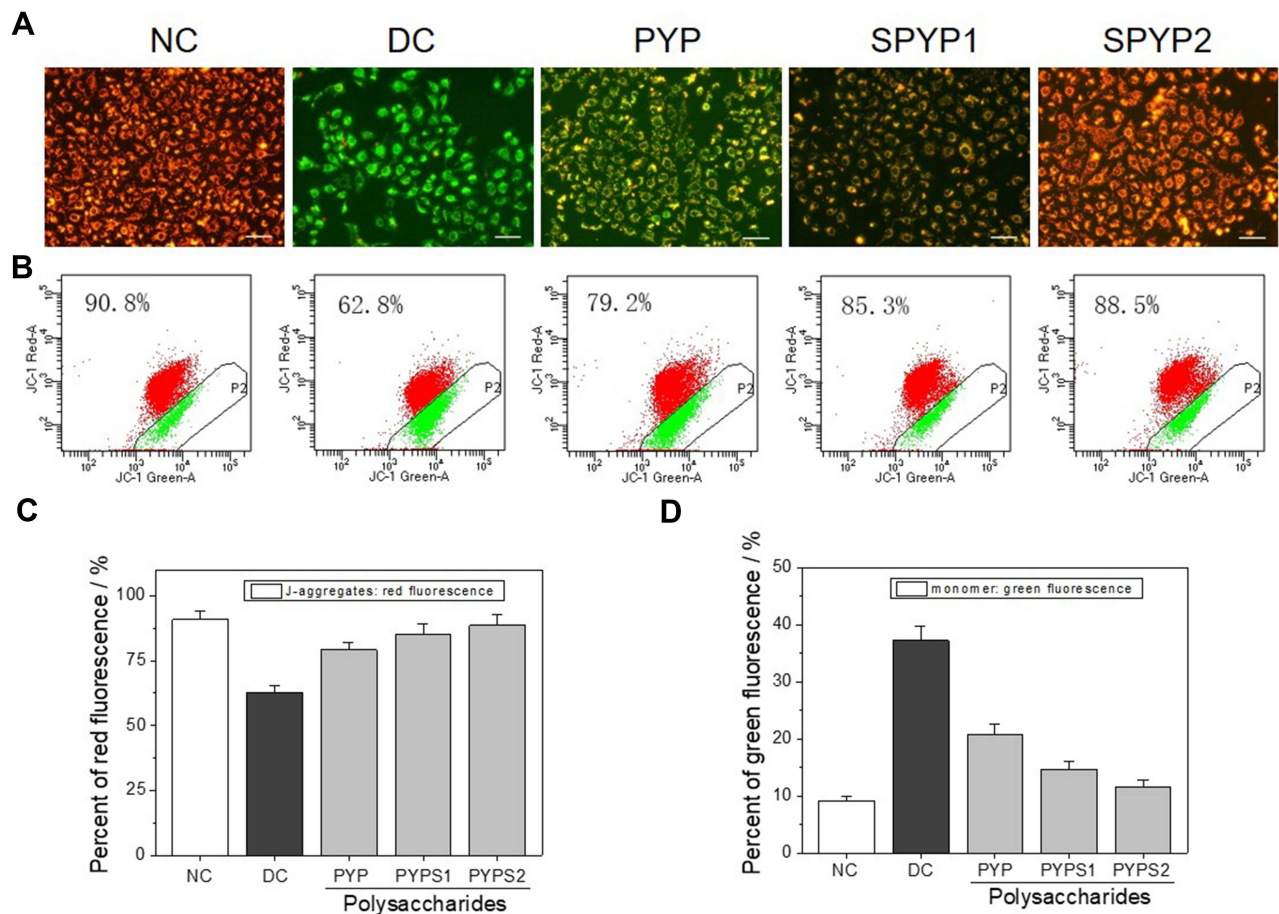


Figure 5 Changes of cell mitochondrial membrane potential of damaged cells before and after repair by PYPs with different $-OSO_3^-$ content. **(A)** Fluorescence microscopy images; **(B)** flow cytometry results; **(C)** quantitative histogram of red fluorescence intensity; **(D)** quantitative histogram of green fluorescence intensity. Polysaccharide concentration: 100 $\mu\text{g/mL}$; oxalate concentration: 2.6 mmol/L ; injury time: 3.5 h; repair time: 12 h. **Abbreviations:** NC, normal control; DC, damaged control.

decreased, and the expression levels were negatively correlated with the $-OSO_3^-$ content in polysaccharides. That is, the expression of adhesion proteins was the lowest after repair by SPYP2 with the highest sulfate content.

PYP Repair Inhibited the Adhesion and Aggregation of Crystals on the Cell Surface

The adhesion and aggregation of COM crystals (100 nm) on the cell surface were observed by SEM (Figure 7A). In

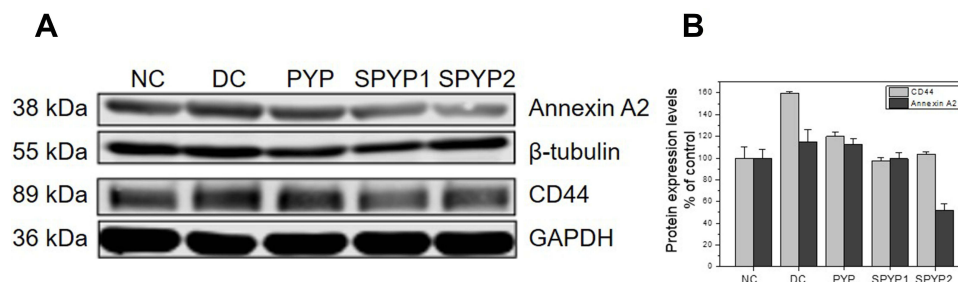


Figure 6 Expression of adhesion proteins of damaged cells before and after repair by PYPs with different $-OSO_3^-$ content. **(A)** Western blotting; **(B)** Quantitative histogram of protein expression. Polysaccharide concentration: 100 $\mu\text{g/mL}$; oxalate concentration: 2.6 mmol/L ; injury time: 3.5 h; repair time: 12 h. **Abbreviations:** NC, normal control; DC, damaged control.

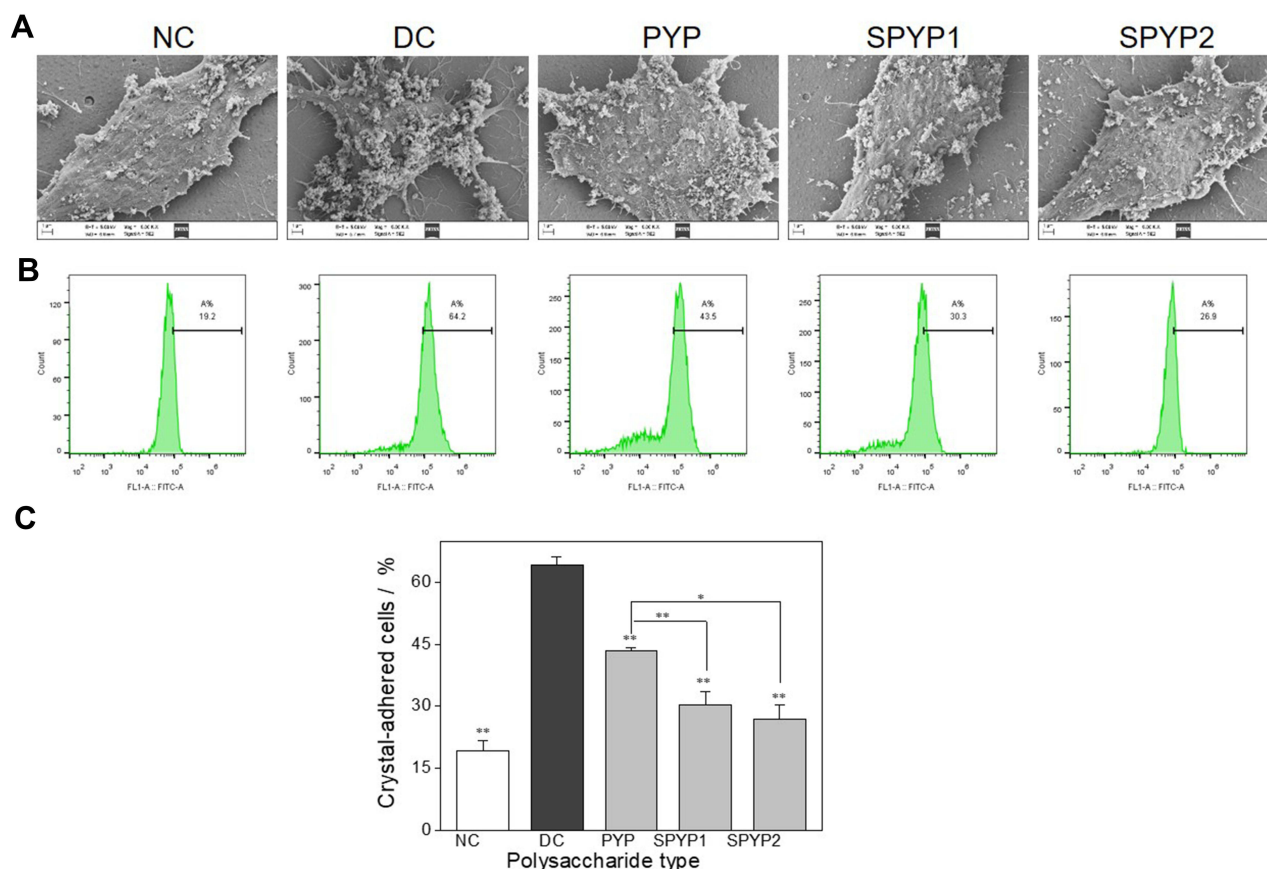


Figure 7 Adhesion of nano-COM crystals on damaged cells before and after repair by PYPs with different $-\text{OSO}_3^-$ content. **(A)** SEM observation; **(B)** quantitative detection of the proportion of cells with adhered FITC-labeled nano-COM crystals by flow cytometry; **(C)** statistical results of the proportion of cells with adhered crystals. Polysaccharide concentration: 100 $\mu\text{g}/\text{mL}$; oxalate concentration: 2.6 mmol/L ; injury time: 3.5 h; repair time: 12 h. Compared with DC group, * $P < 0.05$; ** $P < 0.01$. **Abbreviations:** NC, normal control; DC, damaged control.

the normal group, only a small amount of crystals adhered to the cell surface, and the adhered crystals were almost not aggregated. The cell surface remained smooth and flat after interaction with nano-COM crystals. However, after injury by 2.6 mM oxalate, the cell morphology shrunk, the amount of crystal adhesion was obviously increased, and the degree of crystal aggregation was higher. This finding indicated that the injured cells promoted the adhesion and aggregation of the crystals. After the cells were repaired by various polysaccharides, the amount of crystal adhesion and the degree of aggregation on the cell surface were obviously lower than those of the injured group.

The adhesion of crystals was further quantitatively detected by flow cytometry (Figure 7B). The results showed that the amount of crystal adhesion in the normal group was the lowest (19.2%) (Figure 7C), and that in the injured group, it was the highest (64.2%). The amount of crystal adhesion in the polysaccharide repair group was between normal group and injured group, and it was

negatively correlated with the polysaccharide sulfate content. That is to say, SPYP2 had the strongest ability to inhibit crystal adhesion.

PYP Repair Increased the Endocytosis of Crystals

The crystals adhering to the cell surface can be endocytosed, and then the endocytosed crystals are transferred to the lysosome.³² The accumulation of nano-COM inside cells after polysaccharide repair was observed by a laser confocal microscope (Figure 8A). The normal group had the most orange regions (superposition of green crystals and red lysosomes), indicating that this group contained the most endocytosed crystals. However, the injured group had the least amount of crystal endocytosis. Compared with the injury group, the orange region of each polysaccharide repair group increased to different degrees, which indicated that the ability of endocytosis was enhanced after polysaccharide repair.

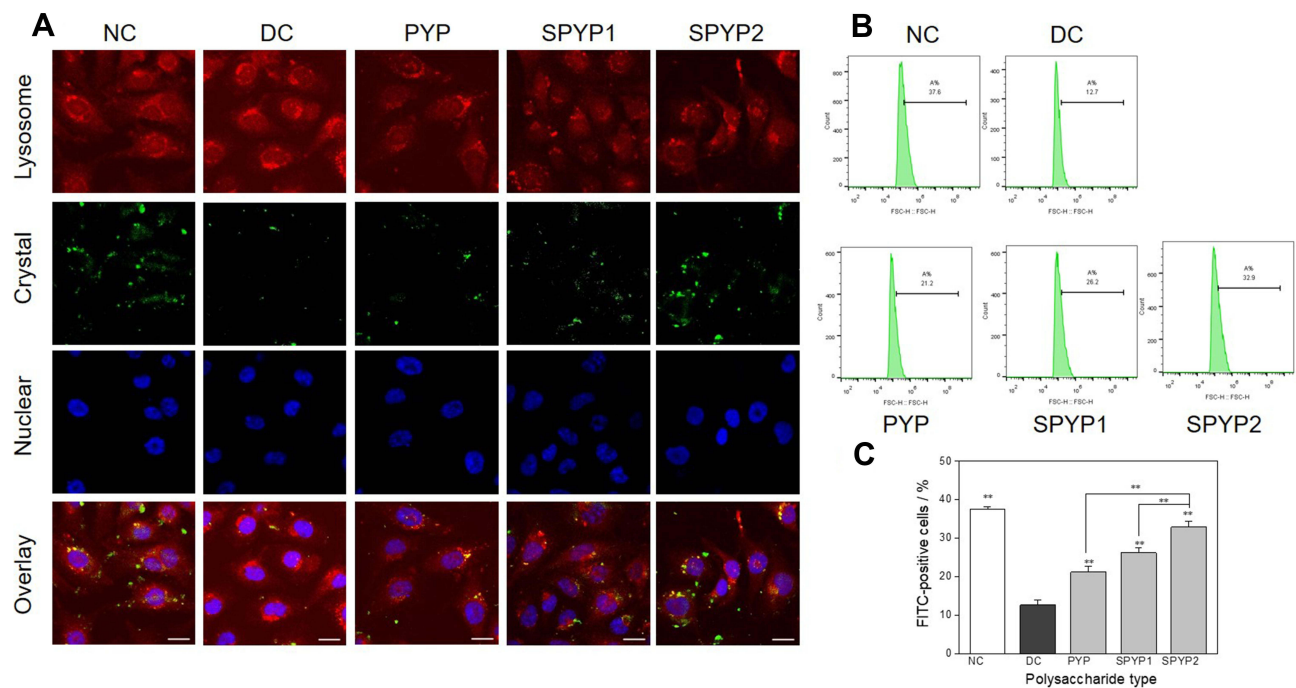


Figure 8 Accumulation of nano-COM crystals in lysosome of damaged cells before and after repair by PYPs with different $-\text{OSO}_3^-$ content. **(A)** Laser confocal observation; **(B)** quantitative detection of the proportion of cells with endocytosed crystals by flow cytometry; **(C)** statistical results of the proportion of cells with endocytosed crystals. Cells were treated with FITC-labeled 200 $\mu\text{g}/\text{mL}$ COM crystals (green fluorescence) for 6 h; lysosomes were stained with Lyso-Tracker Red (red fluorescence); cell nuclei were stained with DAPI (blue fluorescence). Polysaccharide concentration: 100 $\mu\text{g}/\text{mL}$; oxalate concentration: 2.6 mmol/L ; injury time: 3.5 h; repair time: 12 h. Compared with DC group, $**P < 0.01$. Scale: 20 μm .

Abbreviations: NC, normal control; DC, damaged control.

The cells were incubated with 5 mM EDTA for 10 min to eliminate non-internalized (both adherent and non-adherent crystals) COM crystals.²⁴ The internalized FITC labelled-crystals were quantified using a flow cytometer. Cells with an FITC signal, as detected by flow cytometry, can be regarded as cells with endocytosed crystals.³³ The amount of crystal endocytosis was quantitatively determined by flow cytometry (Figure 8B and C). The proportion of cells having endocytosed crystals in the normal group was 37.6%, which was significantly greater than that in the injury group (12.7%, $p < 0.01$). That is, the endocytosis ability of the damaged cells was obviously reduced. After polysaccharide repair, the endocytosis ability of the cells gradually recovered (21.2%–31.9%), and it was positively correlated with the polysaccharide sulfate content.

Discussion

Repair Mechanism of PYPs on Damaged HK-2 Cells

High concentrations of oxalate can produce toxicity to HK-2 cells, promote the production of intracellular ROS, and induce lipid peroxidation.³⁴ ROS can rapidly react with large intracellular molecules (such as proteins,

carbohydrates, and lipids) in cells, resulting in the functional damage to cells and eventually leading to oxidative damage and even cell death.³⁵ Koul et al³⁶ demonstrated that high concentrations of oxalate can lead to a sharp decrease in the number of LLC-PK1 cells and reduced cell viability. Schepers et al³ showed that when the oxalate concentration was more than 5 mmol/L , the release of LDH in MDCK cells was increased, and the levels of H_2O_2 and PGE2 were enhanced. In the present study, oxalate caused the decrease in cell viability (Figure 2A), the disorder of cell morphology (Figure 2B), and the increase of intracellular ROS levels (Figure 3). As a kind of natural antioxidant, plant polysaccharides can clear free radicals and effectively repair oxidative damaged cells.³⁷ Kim et al³⁸ showed that polysaccharides from *Psidium guajava* leaves can reduce H_2O_2 -induced oxidative stress in Vero cells, inhibit lipid peroxidation, and reduce cell oxidative damage. PYP before and after sulfation can effectively improve cell viability, restore cell morphology, and reduce ROS production in cells and oxalate-induced oxidative damage to HK-2 cells.

The $\Delta\psi\text{m}$ of normal cells is higher than that of the damaged cells. Oxalate caused the decrease of $\Delta\psi\text{m}$

(Figure 5), disrupted mitochondrial function, and increased mitochondrial permeability, leading to the release of Ca^{2+} (Figure 4). The increase in Ca^{2+} and lipid peroxidation may be an important factor to cause mitochondrial damage,³⁹ which plays an important role in the formation of kidney stones. Polysaccharides can repair damaged mitochondria. Li et al⁴⁰ reported that *Ganoderma atrum* polysaccharide (PSG-1) increased the expression of Bcl-2 protein in the mitochondria, inhibited the release of cytochrome C, and increased cell $\Delta\psi_m$. Our study showed that PYPs can reduce cell oxidative damage by reducing $\Delta\psi_m$ and Ca^{2+} release. Therefore, PYPs improved cell status, removed ROS in cells, reduced intracellular Ca^{2+} levels, and restored the polarity of mitochondria, leading to the repair of oxalate-damaged HK-2 cells. Our data suggested that PYP repaired the renal cell injury caused by oxalate toxicity by reducing ROS production and inhibiting the reduction of $\Delta\psi_m$ and the release of intracellular Ca^{2+} .

Repairing Damaged Cells Can Inhibit Adhesion and Promote Endocytosis of Crystals

Several studies have shown that the surface of renal epithelial cells has many crystal adhesion proteins and molecules, such as CD44 and annexin A2.^{7,29,30} CD44 is a specific receptor for HA on the cell surface⁴¹ and is also an adhesion protein. Annexin A2 is a calcium-dependent phospholipid-binding protein with a molecular weight of approximately 36 kDa and participates in multiple cellular processes, including cell adhesion, endocytosis, and actin assembly.⁴² The results of this study show that when HK-2 cells are damaged, the three negatively charged adhesion proteins are upregulated (Figure 6). This promotes the adhesion of Ca^{2+} and CaOx crystals to the cell surface, leading to crystal retention and growth and increased risk of stone formation. Verhulst et al⁷ found that renal epithelial cells exposed to CaOx stones have a higher expression of HA and its receptor CD44 than normal cells. Semangoen et al⁴³ proved that the treatment of MDCK cells with 100 $\mu\text{g}/\text{mL}$ COD crystals can significantly increase annexin A2 levels and crystal adhesion.

Polysaccharides have an obvious repair effect on damaged cells, which can restore the morphology and membrane structure of damaged cells to near normal levels.⁴⁴ The results of this study indicate that polysaccharides can reduce the expression of adhesion proteins such as CD44, annexin A2 (Figure 6) and inhibit the

adhesion of crystals. In addition, the cell state is closely related to the amount of crystal adhesion; the better the state, the fewer the cell adhesion sites and the lower the adhesion number of crystals (Figure 7).

Endocytosis is a self-protection mechanism of renal epithelial cells. The adhered crystals are transferred to the lysosome after being endocytosed and dissolved under the action of many hydrolytic enzymes, reducing the toxicity of the crystals.⁴⁵ In the present study, the endocytosis ability of oxalate-damaged cells to nano-COM crystals was obviously reduced (Figure 8B), and the number of crystals accumulated in lysosomes was relatively smaller compared with those of normal cells (Figure 8A). The uptake capacity of repaired cells by PYPs to nano-COM crystals was obviously increased. This is probably because endocytosis is a process of active transportation, which requires the consumption of energy. Cells in good condition have high metabolism and sufficient energy,⁴⁶ and it is easier to endocytose crystals that adhered to the cell surface, reducing the harm of crystal adhesion on the cell surface.

Urine microcrystals cannot grow to a large enough size to block the renal tubules in a short time; however, crystal aggregation can occur in a short period of time. Therefore, the accumulation of crystals is an important factor leading to the retention of crystals in the kidney.⁴⁷ Some studies showed that patients with renal stones secrete more crystal aggregates, which are related to the decrease in stone inhibitors (such as citrate and glycoprotein) and the increase in promoters (such as cell debris, lipid vesicles, and bacteria).^{48,49} Figure 7A shows that the degree of crystal aggregation on the damaged cell surface is obviously higher than that in the polysaccharide repair group, indicating that PYPs have the ability to inhibit the aggregation of urine microcrystals.

Figure 9 shows a model of the adhesion and endocytosis of nano-COM crystals in damaged HK-2 cells before and after repair by PYPs. On the one hand, after PYP repair of damaged cells, the cell viability is enhanced, the cell morphology is restored, the production of ROS is reduced, and the damaged cells are repaired. On the other hand, the reduction of adhesion molecules inhibits the adhesion and aggregation of crystals on the cell surface, promotes the endocytosis of crystals, and reduces the toxicity of cells.

In summary, the adhesion, aggregation, and endocytosis of crystals are closely related to the state of cells. Reducing the adhesion and aggregation of crystals and

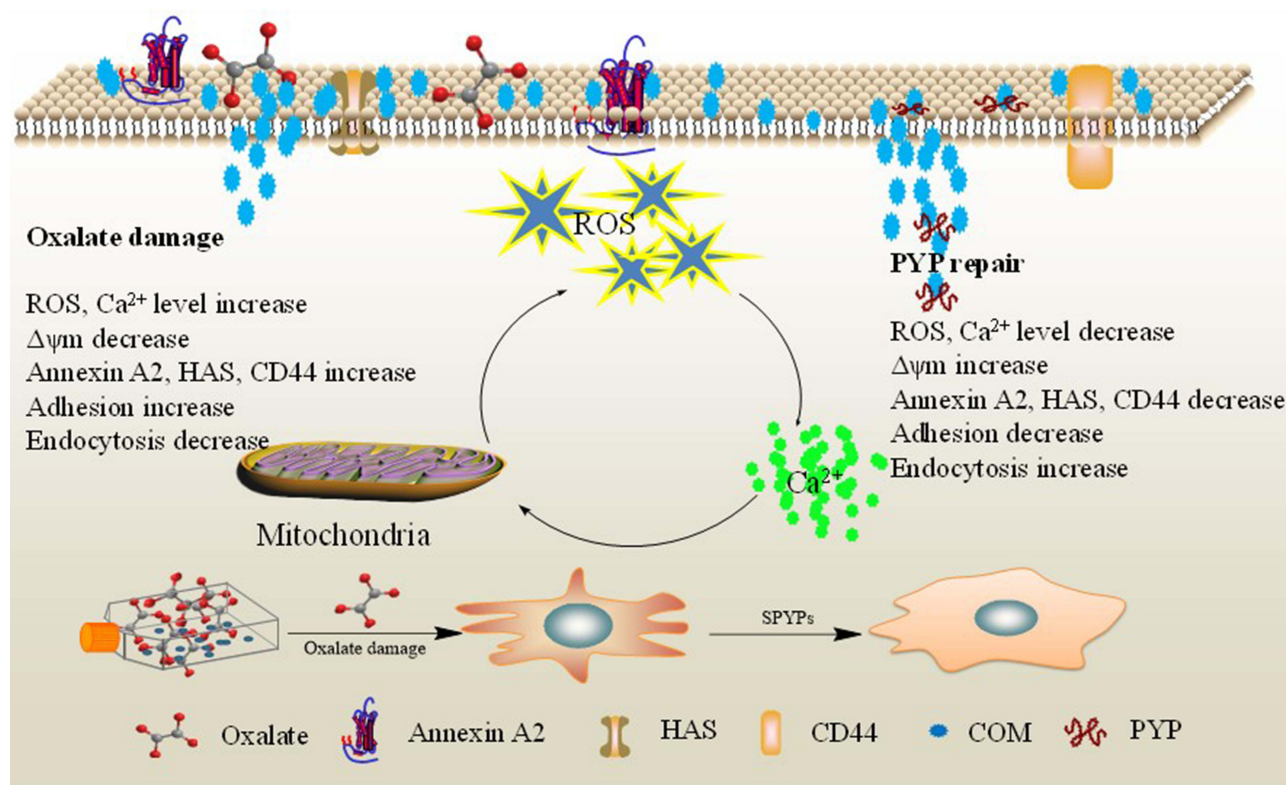


Figure 9 Mechanism of adhesion and endocytosis of nano-COM crystals in damaged HK-2 cells before and after repair by PYPs with different $-\text{OSO}_3^-$ content.

promoting the endocytosis of crystals are effective ways to inhibit the formation of kidney stones.

Sulfation of Polysaccharides Helps to Improve Their Biological Activity

In this study, two sulfated polysaccharides with $-\text{OSO}_3^-$ group contents of 20.28% (SPYP1) and 27.14% (SPYP2) were obtained by sulfating PYP (14.14%) with sulfur trioxide-pyridine for 8 and 16 h, respectively. FT-IR and NMR showed that sulfation did not remarkably affect the overall structure of polysaccharides.

Many studies have shown that the biological activity of sulfated polysaccharides is mainly related to sulfate content.^{50,51} Song et al⁵¹ extracted three kinds of sulfated polysaccharides with $-\text{OSO}_3^-$ contents of 7.56% (B1), 6.71% (B2), and 11.4% (B3) from feather algae and found that B3 had the strongest scavenging ability to superoxide anion and DPPH radicals. Wang et al⁵⁰ showed that 100 $\mu\text{g}/\text{mL}$ of sulfated *Cyclocarya paliurus* polysaccharide could increase the viability of H_2O_2 -damaged macrophages from 60% to 90%. Sun et al⁵² degraded marine microalgae to obtain three polysaccharides with $-\text{OSO}_3^-$ contents of

14.0%, 17.3%, and 25.4% and inhibitory ability against H_2O_2 -induced erythrocyte hemolysis.

The results showed that the repair ability of polysaccharides to damaged HK-2 cells was directly proportional to their $-\text{OSO}_3^-$ group content. Negatively charged $-\text{OSO}_3^-$ in polysaccharides can reduce the negative charge loss on the cell surface and repair the charge barrier.⁵³ Compared with natural PYP, sulfated SPYP has stronger antioxidant activity and can lower ROS levels. The antioxidant ability of polysaccharides is mainly due to their hydrogen supply ability. Hydrogen combines with free radicals and forms stable free radicals to terminate the free radical chain reaction. PYP containing higher $-\text{OSO}_3^-$ content has a stronger ability to activate the hydrogen atoms of anomeric carbon and enhance the donor ability of hydrogen atoms.⁵⁴

As with most polysaccharides, PYP is composed of sugar chains formed by the combination of a variety of monosaccharides through glycosidic bonds. Most polysaccharides have similarities in pharmacokinetics in the body. Many researchers have studied the pharmacokinetics of polysaccharides, and confirmed that polysaccharides can reach the kidney to exert biological activity.^{55–58}

For example, Dawes et al⁵⁷ administered dermatan sulphate to healthy human volunteers by the intravenous, subcutaneous and oral routes, the intact form of dermatan sulphate was subsequently excreted unchanged in the urine. Odland et al⁵⁸ studied the distribution in rats of tritiated sulphated polysaccharide pentosanpolysulphate (PPS) after intravenous injection (5 mg/kg b.wt.) for 1 h. The highest activity in the body was found in the urine as well as in the linings of the renal pelvis, ureter and bladder. Fukatani et al⁵⁶ tested the pharmacokinetics and the changes in crystallization inhibitory capacity for pentosan polysulphate (SP-54) in small groups of healthy volunteers. After oral administration of SP-54, 1% to 2% is excreted unaltered in the urine. Desired increases in urine inhibitory potential against CaOx crystallization were found. In addition, Zhang et al⁵⁵ extracted and isolated PYP by hot-water extract method and studied anti-oxidant activity in aging mice, PYP presented obvious antioxidant capacity in vivo, but detail pharmacokinetic of PYP has not deeply studied.

There are some limitations to our study, which are worth mentioning. First, the molecular mechanism of PYP repairing damaged renal epithelial cells need to be explored in depth. Secondly, in the present study, we just did an in vitro study, so further in vivo and clinical verification is necessary. Thirdly, the detail pharmacokinetics of PYP in vivo need to be further investigated.

Conclusions

PYP before and after sulfation has repair effect on damaged HK-2 cells, and its repair ability is positively correlated with the sulfation degree of polysaccharides. With increased $-\text{OSO}_3^-$ content in polysaccharides, the viability of the repaired cells increases, the amount of ROS decreases, and the reduction of $\Delta\psi_m$ and the release of intracellular Ca^{2+} are suppressed. The abilities of repaired cells to resist crystal adhesion and promote crystal endocytosis were obviously higher than those of injured cells, which was beneficial to reduce the risk of CaOx kidney stone formation. With the highest sulfate content, SPYP2 showed the strongest repair and anti-calculus abilities and may become a potential drug for inhibiting the formation and recurrence of CaOx stones.

Acknowledgment

This work was granted by the National Natural Science Foundation of China (Nos: 21701050 & 21975105) and Guangdong Provincial Science and Technology Plan Project (No. 2017B030314108).

Disclosure

The authors declare that they have no competing interests.

References

- Kang J, Sun Y, Deng Y, et al. Autophagy-endoplasmic reticulum stress inhibition mechanism of superoxide dismutase in the formation of calcium oxalate kidney stones. *Biomed Pharmacother.* 2020;121:109649. doi:10.1016/j.biopha.2019.109649
- Peerapen P, Thongboonkerd V. Protective roles of trigonelline against oxalate-induced epithelial-to-mesenchymal transition in renal tubular epithelial cells: an in vitro study. *Food Chem Toxicol.* 2020;135:110915. doi:10.1016/j.fct.2019.110915
- Schepers MS, van Ballegooijen ES, Bangma CH, Verkoelen CF. Oxalate is toxic to renal tubular cells only at supraphysiologic concentrations. *Kidney Int.* 2005;68(4):1660–1669. doi:10.1111/j.1523-1755.2005.00576.x
- Lieske JC, Norris R, Swift H, Toback FG. Adhesion, internalization and metabolism of calcium oxalate monohydrate crystals by renal epithelial cells. *Kidney Int.* 1997;52(5):1291–1301. doi:10.1038/ki.1997.454
- Lieske JC, Walsh-Reitz MM, Toback FG. Calcium oxalate monohydrate crystals are endocytosed by renal epithelial cells and induce proliferation. *Am J Physiol.* 1992;262(4 Pt 2):F622–F630.
- Zhu C, Liang Q, Liu Y, et al. Kidney injury in response to crystallization of calcium oxalate leads to rearrangement of the intrarenal T cell receptor delta immune repertoire. *J Transl Med.* 2019;17(1):278. doi:10.1186/s12967-019-2022-0
- Verhulst A, Asselman M, Persy VP, et al. Crystal retention capacity of cells in the human nephron: involvement of CD44 and its ligands hyaluronic acid and osteopontin in the transition of a crystal binding-into a nonadherent epithelium. *J Am Soc Nephrol.* 2003;14(1):107–115. doi:10.1097/01.ASN.0000038686.17715.42
- Zhang H, Sun XY, Ouyang JM. Effects of porphyra yezeensis polysaccharide with different molecular weights on the adhesion and endocytosis of nanocalcium oxalate monohydrate in repairing damaged HK-2 cells. *ACS Biomater Sci Eng.* 2019;5(8):3974–3986.
- Zhao YW, Guo D, Li CY, Ouyang JM. Comparison of the adhesion of calcium oxalate monohydrate to HK-2 cells before and after repair using tea polysaccharides. *Int J Nanomedicine.* 2019;14:4277–4292. doi:10.2147/IJN.S198644
- Schmid SL, Carter LL. ATP is required for receptor-mediated endocytosis in intact cells. *J Cell Biol.* 1990;111(6 Pt 1):2307–2318. doi:10.1083/jcb.111.6.2307
- AlKahtane AA, Abushouk AI, Mohammed ET, et al. Fucoïdan alleviates microcystin-LR-induced hepatic, renal, and cardiac oxidative stress and inflammatory injuries in mice. *Environ Sci Pollut Res Int.* 2020;27(3):2935–2944. doi:10.1007/s11356-019-06931-z
- Kim IH, Choi JW, Nam TJ. PYP1-4 peptide from *Pyropia yezeensis* protects against Acetaminophen-induced hepatotoxicity in HepG2 cells. *Exp Ther Med.* 2020;19(2):849–860.
- Sun XY, Zhang H, Liu J, Ouyang JM. Repair activity and crystal adhesion inhibition of polysaccharides with different molecular weights from red algae *Porphyra yezeensis* against oxalate-induced oxidative damage in renal epithelial cells. *Food Funct.* 2019;10(7):3851–3867. doi:10.1039/C8FO02556H
- Ben Abdallah Kolsi R, Bkhairia I, Gargouri L, et al. Protective effect of *Sargassum vulgare* sulfated polysaccharide against molecular, biochemical and histopathological damage caused by alloxan in experimental diabetic rats. *Int J Biol Macromol.* 2017;105(Pt 1):598–607. doi:10.1016/j.ijbiomac.2017.07.079
- Zhao X, Xue CH, Li BF. Study of antioxidant activities of sulfated polysaccharides from *Laminaria japonica*. *J Appl Phycol.* 2008;20(4):431–436. doi:10.1007/s10811-007-9282-4

16. Ma XT, Sun XY, Yu K, Gui BS, Gui Q, Ouyang JM. Effect of content of sulfate groups in seaweed polysaccharides on antioxidant activity and repair effect of subcellular organelles in injured HK-2 cells. *Oxid Med Cell Longev*. 2017;2017:2542950. doi:10.1155/2017/2542950
17. Wang J, Zhang Q, Zhang Z, Li Z. Antioxidant activity of sulfated polysaccharide fractions extracted from *Laminaria japonica*. *Int J Biol Macromol*. 2008;42(2):127–132. doi:10.1016/j.ijbiomac.2007.10.003
18. Zhang H, Sun XY, Chen XW, Ouyang JM. Degraded *Porphyra yezoensis* polysaccharide protects HK-2 cells and reduces nano-COM crystal toxicity, adhesion and endocytosis. *J Mater Chem B*. 2020;8(32):7233–7252. doi:10.1039/D0TB00360C
19. Sun XY, Ouyang JM, Liu AJ, Ding YM, Gan QZ. Preparation, characterization, and in vitro cytotoxicity of COM and COD crystals with various sizes. *Mater Sci Eng C Mater Biol Appl*. 2015;57:147–156. doi:10.1016/j.msec.2015.07.032
20. Chen X-W, Huang W-B, Sun X-Y, Xiong P, Ouyang J-M. Antioxidant activity of sulfated *Porphyra yezoensis* polysaccharides and their regulating effect on calcium oxalate crystal growth. *Mater Sci Eng C*. 2021;128:112338. doi:10.1016/j.msec.2021.112338
21. Tamada Y. Sulfation of silk fibroin by chlorosulfonic acid and the anticoagulant activity. *Biomaterials*. 2004;25(3):377–383. doi:10.1016/S0142-9612(03)00533-7
22. Sakthivel R, Pandima Devi K. Evaluation of physicochemical properties, proximate and nutritional composition of *Gracilaria edulis* collected from Palk Bay. *Food Chem*. 2015;174:68–74. doi:10.1016/j.foodchem.2014.10.142
23. Zhao X, Ng S, Heng BC, et al. Cytotoxicity of hydroxyapatite nanoparticles is shape and cell dependent. *Arch Toxicol*. 2013;87(6):1037–1052. doi:10.1007/s00204-012-0827-1
24. Hovda KE, Guo C, Austin R, McMartin KE. Renal toxicity of ethylene glycol results from internalization of calcium oxalate crystals by proximal tubule cells. *Toxicol Lett*. 2010;192(3):365–372. doi:10.1016/j.toxlet.2009.11.013
25. Zhang Q, Qi H, Zhao T, et al. Chemical characteristics of a polysaccharide from *Porphyra capensis* (Rhodophyta). *Carbohydr Res*. 2005;340(15):2447–2450. doi:10.1016/j.carres.2005.08.009
26. Immanuel G, Sivagnanamurugan M, Marudhupandi T, Radhakrishnan S, Palavesam A. The effect of fucoidan from brown seaweed *Sargassum wightii* on WSSV resistance and immune activity in shrimp *Penaeus monodon* (Fab). *Fish Shellfish Immunol*. 2012;32(4):551–564. doi:10.1016/j.fsi.2012.01.003
27. Yu X, Zhou C, Yang H, et al. Effect of ultrasonic treatment on the degradation and inhibition cancer cell lines of polysaccharides from *Porphyra yezoensis*. *Carbohydr Polym*. 2015;117:650–656. doi:10.1016/j.carbpol.2014.09.086
28. Chen S, Wang J, Xue C, et al. Sulfation of a squid ink polysaccharide and its inhibitory effect on tumor cell metastasis. *Carbohydr Polym*. 2010;81(3):560–566. doi:10.1016/j.carbpol.2010.03.009
29. Verkoelen CF, Van Der Boom BG, Romijn JC. Identification of hyaluronan as a crystal-binding molecule at the surface of migrating and proliferating MDCK cells. *Kidney Int*. 2000;58(3):1045–1054. doi:10.1046/j.1523-1755.2000.00262.x
30. Kumar V, Farell G, Deganello S, Lieske JC. Annexin II is present on renal epithelial cells and binds calcium oxalate monohydrate crystals. *J Am Soc Nephrol*. 2003;14(2):289–297. doi:10.1097/01.ASN.0000046030.24938.0A
31. Asselman M, Verhulst A, De Broe ME, Verkoelen CF. Calcium oxalate crystal adherence to hyaluronan-, osteopontin-, and CD44-expressing injured/regenerating tubular epithelial cells in rat kidneys. *J Am Soc Nephrol*. 2003;14(12):3155–3166. doi:10.1097/01.ASN.0000099380.18995.F7
32. Wu CY, Wu YF, Jin Y, et al. Endosomal/lysosomal location of organically modified silica nanoparticles following caveolae-mediated endocytosis. *RSC Adv*. 2019;9(24):13855–13862. doi:10.1039/C9RA00404A
33. Chaiyarit S, Mungdee S, Thongboonkerd V. Non-radioactive labeling of calcium oxalate crystals for investigations of crystal-cell interactions and internalization. *Anal Methods*. 2010;2(10):1536–1541. doi:10.1039/C0AY00321B
34. Han J, Guo D, Sun XY, Wang JM, Ouyang JM, Gui BS. Repair effects of astragalus polysaccharides with different molecular weights on oxidatively damaged HK-2 cells. *Sci Rep*. 2019;9(1):9871. doi:10.1038/s41598-019-46264-y
35. Huang X, Teng X, Chen D, Tang F, He J. The effect of the shape of mesoporous silica nanoparticles on cellular uptake and cell function. *Biomaterials*. 2010;31(3):438–448. doi:10.1016/j.biomaterials.2009.09.060
36. Koul H, Kennington L, Nair G, Honeyman T, Menon M, Scheid C. Oxalate-induced initiation of DNA synthesis in LLC-PK1 cells, a line of renal epithelial cells. *Biochem Biophys Res Commun*. 1994;205(3):1632–1637. doi:10.1006/bbrc.1994.2854
37. Bhadja P, Lunagariya J, Ouyang JM. Seaweed sulphated polysaccharide as an inhibitor of calcium oxalate renal stone formation. *J Funct Foods*. 2016;27:685–694. doi:10.1016/j.jff.2016.10.016
38. Kim SY, Kim EA, Kim YS, et al. Protective effects of polysaccharides from *Psidium guajava* leaves against oxidative stresses. *Int J Biol Macromol*. 2016;91:804–811. doi:10.1016/j.ijbiomac.2016.05.111
39. Hu S, Wang D, Zhang J, et al. Mitochondria related pathway is essential for polysaccharides purified from *sparassis crispa* mediated neuro-protection against glutamate-induced toxicity in differentiated PC12 cells. *Int J Mol Sci*. 2016;17(2):133. doi:10.3390/ijms17020133
40. Li WJ, Nie SP, Yao YF, et al. *Ganoderma atrum* polysaccharide ameliorates hyperglycemia-induced endothelial cell death via a mitochondria-ROS pathway. *J Agric Food Chem*. 2015;63(37):8182–8191. doi:10.1021/acs.jafc.5b03462
41. Weber GF, Ashkar S, Glimcher MJ, Cantor H. Receptor-ligand interaction between CD44 and osteopontin (Eta-1). *Science*. 1996;271(5248):509–512. doi:10.1126/science.271.5248.509
42. Sorokina EA, Kleinman JG. Cloning and preliminary characterization of a calcium-binding protein closely related to nucleolin on the apical surface of inner medullary collecting duct cells. *J Biol Chem*. 1999;274(39):27491–27496. doi:10.1074/jbc.274.39.27491
43. Semangoen T, Sinchaikul S, Chen ST, Thongboonkerd V. Altered proteins in MDCK renal tubular cells in response to calcium oxalate dihydrate crystal adhesion: a proteomics approach. *J Proteome Res*. 2008;7(7):2889–2896. doi:10.1021/pr800113k
44. Li Q, Yang H, Wang W, et al. Brassica rapa polysaccharides ameliorate CCl4-induced acute liver injury in mice through inhibiting inflammatory apoptotic response and oxidative stress. *Chem Biodivers*. 2020;17(1):e1900534. doi:10.1002/cbdv.201900534
45. Li X, He Q, Shi J. Global gene expression analysis of cellular death mechanisms induced by mesoporous silica nanoparticle-based drug delivery system. *ACS Nano*. 2014;8(2):1309–1320. doi:10.1021/nn4046985
46. Patel M, Yarlagadda V, Adedoyin O, et al. Oxalate induces mitochondrial dysfunction and disrupts redox homeostasis in a human monocyte derived cell line. *Redox Biol*. 2018;15:207–215. doi:10.1016/j.redox.2017.12.003
47. Chutipongtanate S, Sutthimethakorn S, Chiangjong W, Thongboonkerd V. Bacteria can promote calcium oxalate crystal growth and aggregation. *J Biol Inorg Chem*. 2013;18(3):299–308. doi:10.1007/s00775-012-0974-0
48. Baumann JM, Affolter B, Casella R. Aggregation of freshly precipitated calcium oxalate crystals in urine of calcium stone patients and controls. *Urol Res*. 2011;39(6):421–427. doi:10.1007/s00240-011-0382-x
49. Nakagawa Y, Abram V, Parks JH, Lau HS, Kawooya JK, Coe FL. Urine glycoprotein crystal growth inhibitors. Evidence for a molecular abnormality in calcium oxalate nephrolithiasis. *J Clin Invest*. 1985;76(4):1455–1462. doi:10.1172/JCI112124

50. Wang ZJ, Xie JH, Kan LJ, et al. Sulfated polysaccharides from *Cyclocarya paliurus* reduce H₂O₂-induced oxidative stress in RAW264.7 cells. *Int J Biol Macromol.* 2015;80:410–417. doi:10.1016/j.ijbiomac.2015.06.031
51. Song HF, Zhang QB, Zhang ZS, Wang J. In vitro antioxidant activity of polysaccharides extracted from *Bryopsis plumosa*. *Carbohydr Polym.* 2010;80(4):1057–1061. doi:10.1016/j.carbpol.2010.01.024
52. Sun L, Wang L, Li J, Liu H. Characterization and antioxidant activities of degraded polysaccharides from two marine Chrysophyta. *Food Chem.* 2014;160:1–7. doi:10.1016/j.foodchem.2014.03.067
53. Yao XQ, Ouyang JM, Peng H, Zhu WY, Chen HQ. Inhibition on calcium oxalate crystallization and repair on injured renal epithelial cells of degraded soybean polysaccharide. *Carbohydr Polym.* 2012;90(1):392–398. doi:10.1016/j.carbpol.2012.05.056
54. Chen HX, Zhang M, Qu ZS, Xie BJ. Antioxidant activities of different fractions of polysaccharide conjugates from green tea (*Camellia Sinensis*). *Food Chem.* 2008;106(2):559–563. doi:10.1016/j.foodchem.2007.06.040
55. Zhang Q, Li N, Liu X, Zhao Z, Li Z, Xu Z. The structure of a sulfated galactan from *Porphyra haitanensis* and its in vivo antioxidant activity. *Carbohydr Res.* 2004;339(1):105–111. doi:10.1016/j.carres.2003.09.015
56. Fukatani T. [Studies of sodium pentosan polysulphate (SPP) therapy on the urinary stone disease. Experimental studies on the calcium oxalate crystallization and the effects in healthy subjects]. *Nihon Hinyokika Gakkai Zasshi.* 1991;82(2):246–253. Japanese.
57. Dawes J, Hodson BA, Pepper DS. The absorption, clearance and metabolic fate of dermatan sulphate administered to man—studies using a radioiodinated derivative. *Thromb Haemost.* 1989;62(3):945–949. doi:10.1055/s-0038-1651033
58. Odland B, Dencker L, Tengblad A. Preferential localization of 3H-pentosanpolysulphate to the urinary tract in rats. *Pharmacol Toxicol.* 1987;61(3):162–166. doi:10.1111/j.1600-0773.1987.tb01796.x

International Journal of Nanomedicine

Dovepress

Publish your work in this journal

The International Journal of Nanomedicine is an international, peer-reviewed journal focusing on the application of nanotechnology in diagnostics, therapeutics, and drug delivery systems throughout the biomedical field. This journal is indexed on PubMed Central, MedLine, CAS, SciSearch®, Current Contents®/Clinical Medicine,

Journal Citation Reports/Science Edition, EMBase, Scopus and the Elsevier Bibliographic databases. The manuscript management system is completely online and includes a very quick and fair peer-review system, which is all easy to use. Visit <http://www.dovepress.com/testimonials.php> to read real quotes from published authors.

Submit your manuscript here: <https://www.dovepress.com/international-journal-of-nanomedicine-journal>